



Immobilized manganese porphyrin on functionalized magnetic nanoparticles via axial ligation: efficient and recyclable nanocatalyst for oxidation reactions

Mojtaba Bagherzadeh & Anahita Mortazavi-Manesh

To cite this article: Mojtaba Bagherzadeh & Anahita Mortazavi-Manesh (2015) Immobilized manganese porphyrin on functionalized magnetic nanoparticles via axial ligation: efficient and recyclable nanocatalyst for oxidation reactions, *Journal of Coordination Chemistry*, 68:13, 2347-2360, DOI: [10.1080/00958972.2015.1046850](https://doi.org/10.1080/00958972.2015.1046850)

To link to this article: <http://dx.doi.org/10.1080/00958972.2015.1046850>



Accepted author version posted online: 05 May 2015.
Published online: 02 Jun 2015.



Submit your article to this journal [↗](#)



Article views: 71



View related articles [↗](#)



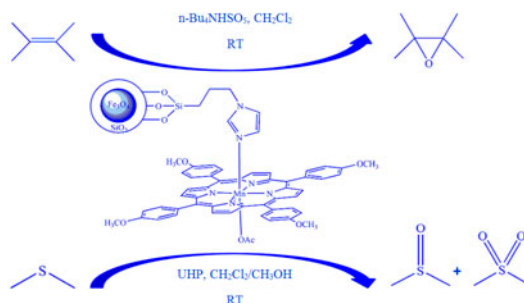
View Crossmark data [↗](#)

Immobilized manganese porphyrin on functionalized magnetic nanoparticles via axial ligation: efficient and recyclable nanocatalyst for oxidation reactions

MOJTABA BAGHERZADEH* and ANAHITA MORTAZAVI-MANESH

Chemistry Department, Sharif University of Technology, Tehran, Iran

(Received 26 November 2014; accepted 13 April 2015)



Magnetic nanoparticles (MNPs), $\text{Fe}_3\text{O}_4@\text{SiO}_2$, have been prepared and functionalized by 3-(chloropropyl)trimethoxysilane and then by imidazole to synthesize $\text{Fe}_3\text{O}_4@\text{SiO}_2\text{-Im}$. The functionalized Fe_3O_4 nanoparticles were used as a support to anchor manganese porphyrin via axial ligation. The prepared catalyst was characterized by elemental analysis, FT-IR spectroscopy, X-ray powder diffraction, UV–vis spectroscopy, and scanning electron microscopy. Application of immobilized manganese porphyrin as a heterogeneous catalyst in oxidation of alkenes and sulfides was explored. To find suitable reaction conditions, effect of different parameters such as solvent and temperature on immobilization process and also various reaction parameters (oxidant, solvent, and time) on oxidation reactions has been investigated. The results showed that the immobilized Mn-porphyrin on functionalized MNPs is an efficient and reusable catalyst for oxidation of substrates.

Keywords: Magnetic nanoparticles; Surface functionalization; Nanocatalyst; Immobilized manganese porphyrin; Oxidation reactions

1. Introduction

As biomimetic catalysts in oxidation reactions, metalloporphyrin complexes have been employed. Immobilization of metalloporphyrin catalysts on insoluble organic and inorganic supports improves their stability and selectivity because of the support environment and other advantages with respect to recovery and reuse [1–5]. An attractive approach is

*Corresponding author. Email: bagherzadeh@sharif.edu

preparation of the heterogeneous catalyst by immobilization of complexes on silica-coated magnetic nanoparticles. Heterogenized homogeneous catalysts are an attractive option to facilitate separation of catalyst, simplified product workup and continuity of the catalytic system [6]. Although immobilization of a homogeneous catalyst on solid supports facilitates its separation, normally this results in a decrease in the active surface area and reactivity of the catalyst. Homogeneous catalysts immobilized on magnetic nanoparticles (MNPs) occupy a unique position due to combining the advantages of both homogeneous and heterogeneous catalysts [7–9]. In addition, superparamagnetic nature of MNPs enables very simple separation of the immobilized catalysts from the reaction mixture using an external magnet.

In this article, we describe the preparation of imidazole functionalized Fe_3O_4 nanoparticles ($\text{Fe}_3\text{O}_4@\text{SiO}_2\text{-Im}$). These modified particles have been utilized as a support for immobilization of Mn-porphyrin. The catalytic activity of the supported catalyst in the oxidation of alkenes and sulfides and also the effect of different parameters on immobilization process and oxidation reactions have been investigated.

2. Experimental

2.1. Materials and methods

All reagents and solvents were purchased from Aldrich or Merck Chemical Companies. Scanning electron microscopy (SEM) was carried out on a Philips XL30. FT-IR spectra were recorded as KBr pellets using an ABB FT-IR spectrophotometer. Measures of pH were carried out on a Mettler Toledo S40 SevenMulti™ pH-meter. X-ray diffraction (XRD) pattern was obtained by D4 ENDEAVOR diffractometer (Bruker AXS Inc.) with $\text{Cu K}\alpha$ as a radiation source, the scan range (2θ) was from 5° to 100° . A Varian (AA220) flame atomic absorption spectrometer (AAS) (air/acetylene flame) was used for manganese ion determinations. Elemental analyses (CHN) were performed using a Heraeus Elemental Analyzer. UV–vis spectra were recorded with a Shimadzu UV-2100 spectrometer. Gas chromatographic (GC) analyses were performed on an Agilent Technologies 6890 N, 19,019 J-413 HP-5, capillary $60\text{ m} \times 250\ \mu\text{m} \times 1\ \mu\text{m}$.

2.2. Preparation of Fe_3O_4 MNPs

Fe_3O_4 nanoparticles were synthesized according to the procedure described previously [9, 10]. In brief, under N_2 atmosphere, 5.2 g (19.3 mmol) of $\text{FeCl}_3 \cdot 6\text{H}_2\text{O}$, 2 g (10.0 mmol) of $\text{FeCl}_2 \cdot 4\text{H}_2\text{O}$, and 0.85 mL concentrated HCl were dissolved in 25 mL degassed water. This solution was added dropwise at room temperature to 250 mL of NaOH solution (1.5 mol/L) under N_2 . The reaction mixture was vigorously stirred for 30 min (1300 rpm). The formed black precipitates were separated using a strong magnetic field (0.5 T magnet) and washed several times with degassed water. Finally, for storage, Fe_3O_4 nanoparticles were dispersed in 200 mL degassed water under N_2 . Synthesis of Fe_3O_4 nanoparticles was confirmed by XRD.

2.3. Synthesis of $\text{Fe}_3\text{O}_4@\text{SiO}_2$ nanoparticles

In the next step, Fe_3O_4 MNPs were coated with a thin layer of silica [11, 12]. One gram of freshly prepared Fe_3O_4 nanoparticles was added into 30 mL of an aqueous solution of citric acid (0.02 g/mL), then the pH was adjusted to 5.2 using ammonia, and the mixture was

heated to 80–90 °C for 1.5 h. After heating, the pH of the reaction mixture was increased with ammonia to pH 11 and 1.25 mL of tetraethylorthosilicate (TEOS) dissolved in ethanol (12.5 mL) was added dropwise into the suspension of particles. The mixture was stirred at room temperature for 24 h to let the base-catalyzed hydrolysis and condensation of TEOS monomers on the nanoparticle surface go to completion. Finally, the dark brown Fe₃O₄@-SiO₂ nanoparticles were separated using a 0.5 T magnet and were washed with distilled water (5 times, 150 mL) and ethanol (5 times, 150 mL). Synthesis of Fe₃O₄@SiO₂ nanoparticles was confirmed with X-ray diffraction analysis.

2.4. Preparation of imidazole functionalized Fe₃O₄@SiO₂ nanoparticles

In a typical reaction, Fe₃O₄@SiO₂ nanoparticles (1.00 g) were suspended in dried toluene (70 mL). 3-Chloropropyl trimethoxysilane (0.27 mL) was added, and the mixture was refluxed for 24 h. There potassium iodide (0.25 g) was added to the mixture and stirred for 1 h; imidazole (0.20 g) was added, and the mixture was refluxed again for 24 h [13]. The solid phase was filtered and washed with acetone and diethyl ether, respectively, to remove impurities and dried at 120 °C. Functionalization of Fe₃O₄ nanoparticles was confirmed by FT-IR spectroscopy, and elemental analysis (CHN).

2.5. Porphyrin synthesis and metallation

In this work, *meso*-tetrakis(4-methoxyphenyl)porphyrin; [T(4-OMeP)P], was prepared according to the Adler procedure [14] and metallated with Mn(OAc)₂·4H₂O by method of Adler and coworkers to synthesize [MnT(4-OMeP)P]OAc [15].

2.6. Catalyst preparation (immobilization process)

The synthesized Fe₃O₄@SiO₂-Im (0.10 g) was suspended in CH₂Cl₂ (10 mL) containing metalloporphyrin (0.11 mmol). The mixture was refluxed for 24 h, the solid was filtered, washed with CH₂Cl₂ and ethanol and dried at 120 °C for 4 h. The quantity of immobilized manganese porphyrin was determined by measuring the manganese content of the prepared catalyst; Fe₃O₄@SiO₂-Im@[MnT(4-OMeP)P], by AAS.

2.7. General oxidation procedure

A typical oxidation reaction using Fe₃O₄@SiO₂-Im@[MnT(4-OMeP)P] nanoparticles as catalyst is described as follows. In a 10-mL round-bottom flask, the prepared catalyst (0.01 g, containing 7×10^{-4} mmol of MnPor), substrate (0.20 mmol), chlorobenzene (0.20 mmol) as the internal standard and oxidant (0.40 mmol) were added in order with a molar ratio of catalyst:substrate:oxidant of 1:285:570. The reaction mixture was stirred at room temperature in a tightly closed flask. The reaction products were monitored in different time intervals, 3 and 20 h, using GC. The catalyst nanoparticles were collected at the bottom of the round-bottom flask using a magnet, supernatant carefully decanted and formation of products was monitored by GC. The oxidation products were identified by comparison with authentic samples (retention times in GC). An internal standard method was used to calculate yields. All reactions were repeated at least two times.

2.8. Reusability of the catalyst

The reusability and the stability of the prepared catalyst were studied in repeated oxidation reactions. The catalyst was filtered from the reaction mixture after each run and washed with CH_2Cl_2 and then dried in vacuum at room temperature for 4 h before reusing in the subsequent oxidation reaction and could be reused about six times without significant loss of the catalytic activity.

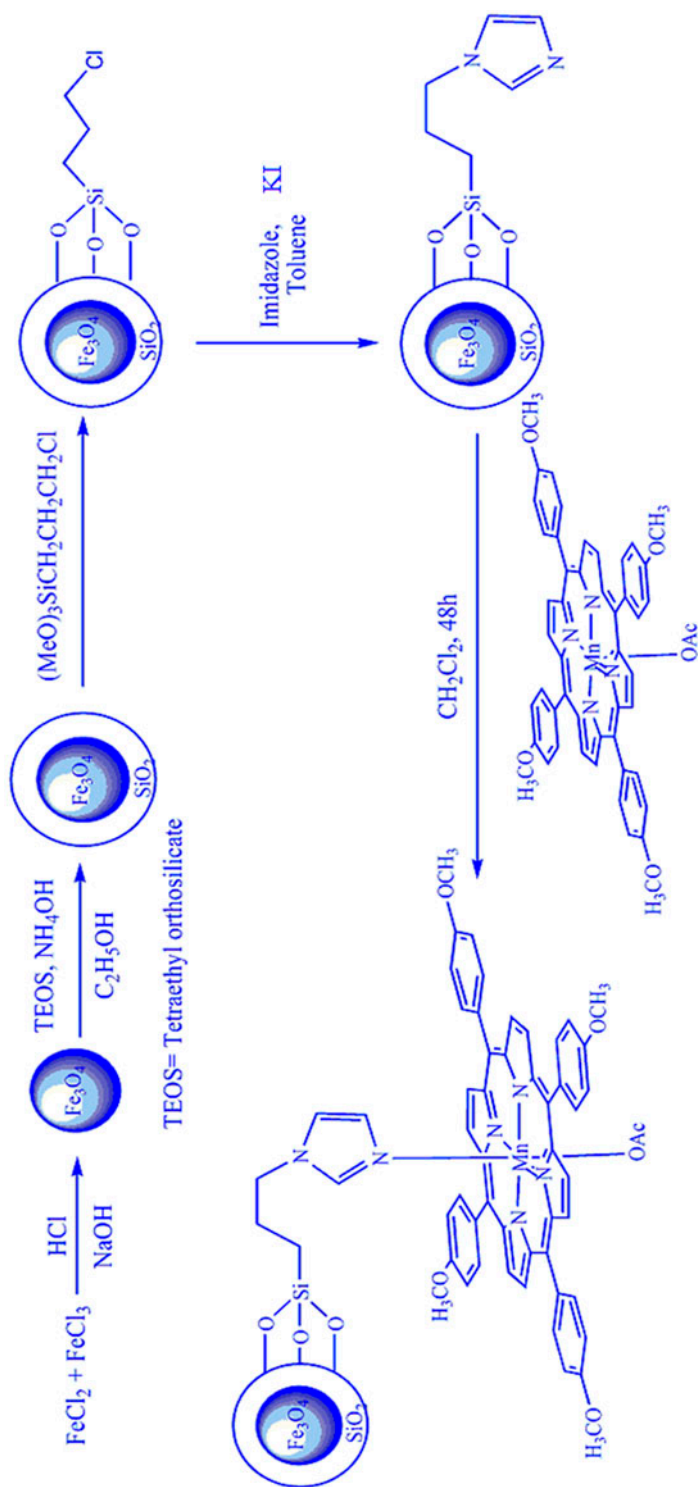
3. Results and discussion

Magnetically separable $\text{Fe}_3\text{O}_4@\text{SiO}_2\text{-Im}@[\text{MnT}(4\text{-OMeP})\text{P}]$ (**1**) catalyst was synthesized by the route schematically demonstrated in scheme 1. In the first step, Fe_3O_4 nanoparticles were prepared using the coprecipitation method. Silica-coated nanoparticles were obtained by hydrolysis and condensation of TEOS on the surface of the Fe_3O_4 nanoparticles. In the next step, $\text{Fe}_3\text{O}_4@\text{SiO}_2$ was functionalized by 3-(chloropropyl)trimethoxysilane and then by imidazole to synthesize $\text{Fe}_3\text{O}_4@\text{SiO}_2\text{-Im}$. The supported catalyst (**1**) was prepared by reaction of $\text{Fe}_3\text{O}_4@\text{SiO}_2\text{-Im}$ with $[\text{MnT}(4\text{-OMeP})\text{P}]\text{OAc}$. By modification of Fe_3O_4 nanoparticles surface with imidazole, imidazole groups on the surface of the functionalized Fe_3O_4 bond to the axial position of the manganese porphyrin. The bonding of the $\text{Fe}_3\text{O}_4@\text{SiO}_2\text{-Im}$ and the metalloporphyrin is so strong that $[\text{MnT}(4\text{-OMeP})\text{P}]\text{OAc}$ is not eluted from the support with common organic solvents.

3.1. Characterization of the catalyst, $\text{Fe}_3\text{O}_4@\text{SiO}_2\text{-Im}@[\text{MnT}(4\text{-OMeP})\text{P}]$

The nitrogen content of $\text{Fe}_3\text{O}_4@\text{SiO}_2\text{-Im}$ was 1.74 mmol/g as measured by CHN analysis. This observation strongly justifies the conclusion that surface functionalization by imidazole has been successful. Based on this value, the amount of available nitrogen for coordination to Mn is 0.87 mmol/g. The manganese content of the supported catalyst as determined by AAS was 0.07 mmol/g of the supported catalyst. Therefore, analysis shows about 8% of the imidazole groups on the surface of Fe_3O_4 nanoparticles were coordinated to the metalloporphyrin.

The XRD patterns for the nanoparticles before and after growing a SiO_2 shell and after immobilization of the catalyst were obtained with X-ray diffraction analysis (figure 1). In the XRD pattern of the prepared Fe_3O_4 [figure 1(a)], six characteristic peaks ($2\theta = 30.6, 35.7, 43.8, 54.2, 57.3,$ and 63.6), corresponding to (220), (311), (400), (422), (511), and (440) Bragg reflections, respectively, were observed. These diffraction peaks are in agreement with the database in JCPDS file (PCPDFWIN v.2.02, PDF No. 85-1436) and reveal that the resultant nanoparticles were pure Fe_3O_4 without impurity phases. This XRD pattern is consistent with the pattern previously reported for Fe_3O_4 samples [16, 17]. The XRD pattern of $\text{Fe}_3\text{O}_4@\text{SiO}_2$ core/shell is shown in figure 1(b). The same characteristic peaks can also be found in this pattern suggesting that the crystalline structure of Fe_3O_4 nanoparticles does not change after the surface modification with silica. However, the weaker intensity in figure 1(b) than that of figure 1(a) can be attributed to shielding of the amorphous silica shell. Also, figure 1 shows the XRD pattern of the MNPs@MPor [figure 1(c)] with characteristic peaks and relative intensity, which completely match with the standard Fe_3O_4

Scheme 1. Step-by-step synthesis of the $\text{Fe}_3\text{O}_4@ \text{SiO}_2\text{-Im@[MnT(4-OMeP)P]}$ catalyst (I).

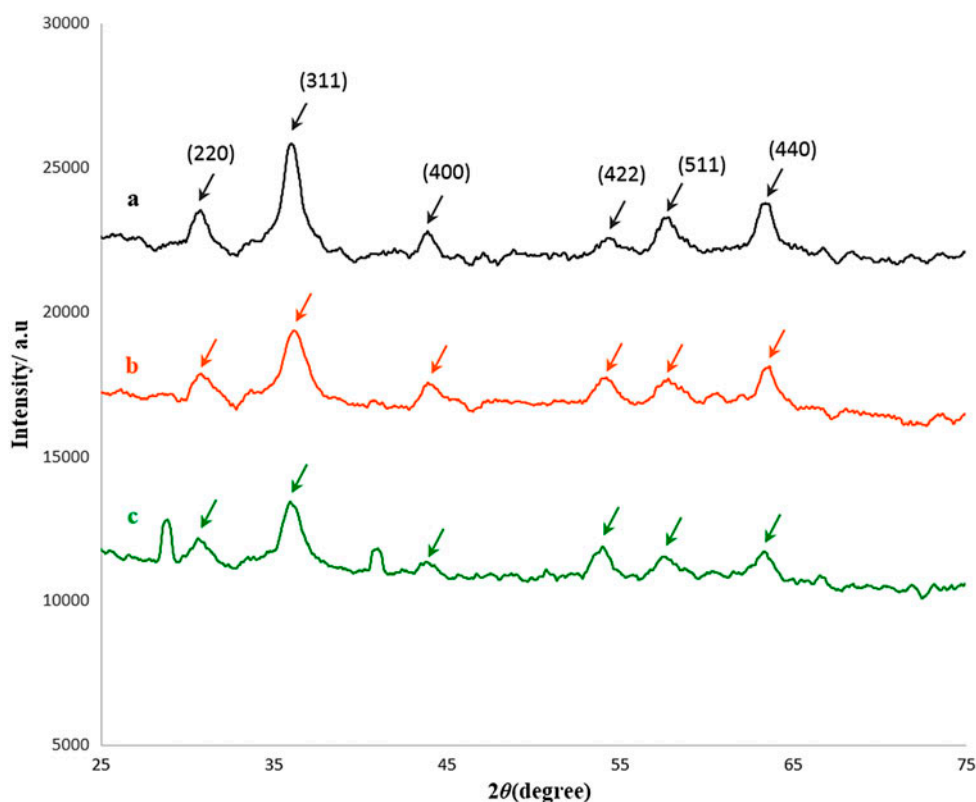


Figure 1. XRD pattern of: (a) Fe₃O₄, (b) Fe₃O₄@SiO₂, and (c) MNPs@MPor: Fe₃O₄@SiO₂-Im@[MnT(4-OMeP)P].

sample. In addition, the average particle size of the immobilized catalyst was estimated by Scherrer's equation to be 24.9, which is in agreement with that observed in the SEM image.

The SEM image of Fe₃O₄@SiO₂-Im@[MnT(4-OMeP)P] nanocatalyst, as shown in figure 2, clearly suggests a smooth morphology of the catalyst; particles were well distributed with dimensions about 33 nm and rather high surface area. The high surface area of nanoparticles is beneficial for high loading of catalyst during the complex anchoring step.

The FT-IR spectroscopy was employed for the characterization of supported catalyst. figure 3 shows FT-IR spectra of the core-shell MNPs (Fe₃O₄@SiO₂) before and after being functionalized by imidazole. The FT-IR spectra of Fe₃O₄@SiO₂ nanoparticles [figure 3(a)] represent significant absorption bands at 593 and 637 cm⁻¹ which corresponds to Fe–O vibrational modes of Fe₃O₄. Furthermore, a strong absorption at 1084 cm⁻¹ (between 1200 and 1000 cm⁻¹) and a band at 802 cm⁻¹, which can be assigned to the Si–O–Si stretching vibrations [18, 19], indicate that the Fe₃O₄ core is coated by a silica layer. Bands at 1631 and 3443 cm⁻¹ are associated with vibrations of absorbed water [20].

Imidazole functionalized nanoparticles (Fe₃O₄@SiO₂-Im) were systematically characterized by FT-IR in addition to elemental analysis. Compared with FT-IR spectra of Fe₃O₄@SiO₂, characteristic peaks at 2863 and 2935 cm⁻¹ ascribed to vibrations of the propyl groups can be clearly observed in FT-IR spectra of Fe₃O₄@SiO₂-Im [figure 3(b)],



Figure 2. The SEM image of $\text{Fe}_3\text{O}_4@SiO_2\text{-Im@[MnT(4-OMeP)P]}$.

confirming that 3-(chloropropyl)trimethoxysilane molecules bonded to the surface of the silica-coated MNPs [21]. Additionally, two C–N vibrations between 1400 and 1600 cm^{-1} [figure 3(b)], become visible after imidazole anchorage. These bands can be attributed to conjugated C=N vibrations of cyclic systems (imidazole), proving imidazole incorporation [22, 23]. As previously mentioned, this conclusion is further supported by elemental analysis. Immobilization of metalloporphyrin on imidazole functionalized nanoparticles was exhibited by FT-IR spectroscopy. Comparing FT-IR spectra of $\text{Fe}_3\text{O}_4@SiO_2\text{-Im}$ and $\text{Fe}_3\text{O}_4@SiO_2\text{-Im@MPor}$ nanoparticles (figure 4), IR spectra of heterogenized manganese porphyrin complex show new peaks at 1172 , 1249 , and 1607 cm^{-1} [figure 4(a)], also observed in the FT-IR spectrum of $[MnT(4-OMeP)P]OAc$ [figure 4(b)]. These peaks belong

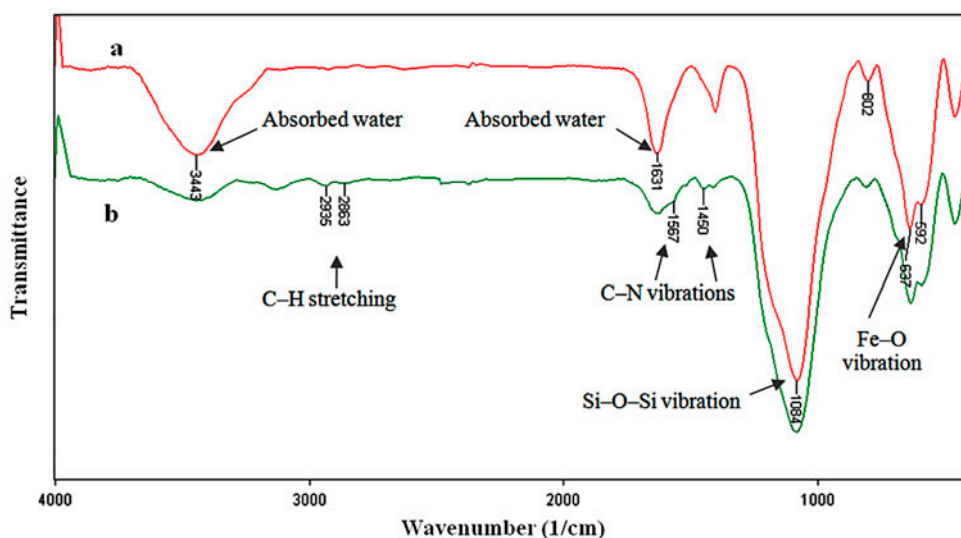


Figure 3. FT-IR spectra of: (a) $\text{Fe}_3\text{O}_4@SiO_2$, (b) $\text{Fe}_3\text{O}_4@SiO_2\text{-Im}$.

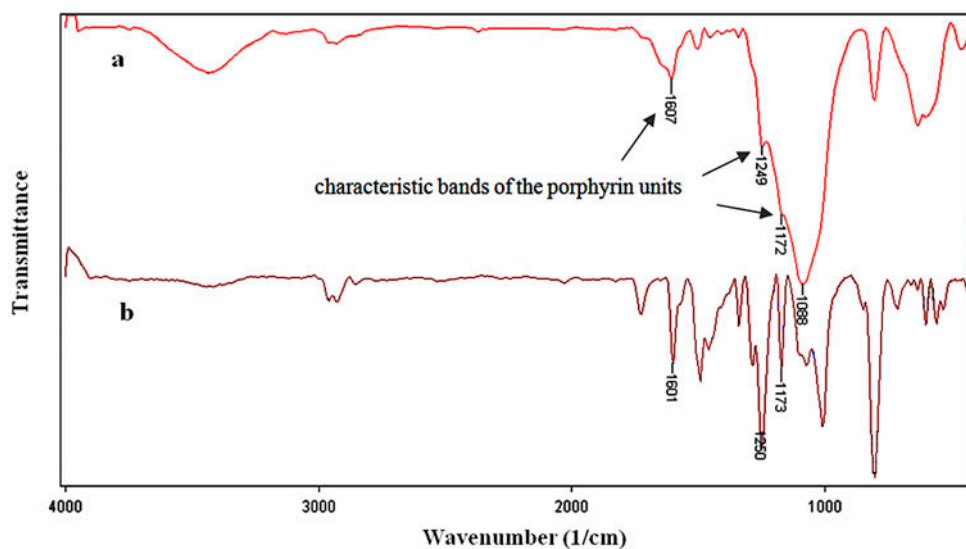


Figure 4. FT-IR spectra of: (a) $\text{Fe}_3\text{O}_4@\text{SiO}_2\text{-Im}@\text{[MnT(4-OMeP)]}$ (1), (b) [MnT(4-OMeP)]OAc .

to the characteristic bands of the porphyrin units at 1172 (C-H_{Ph}), 1249 (C-N), and 1607 (C=N) cm^{-1} [24].

The presence of metalloporphyrin on the functionalized MNPs was also confirmed by UV-vis spectroscopy (figure 5). No absorption band was observed in the UV-vis spectra of $\text{Fe}_3\text{O}_4@\text{SiO}_2\text{-Im}$ [figure 5(a), dash line]. However, the Soret band at 480 nm and Q bands at 583 and 625 nm appear after immobilization of [MnT(4-OMeP)] on the surface [figure 5(b)].

The FT-IR spectrum, coupled with the UV-vis spectroscopy, provides evidence for anchoring of the manganese porphyrin on imidazole functionalized silica-coated Fe_3O_4 nanoparticles via axial ligation.

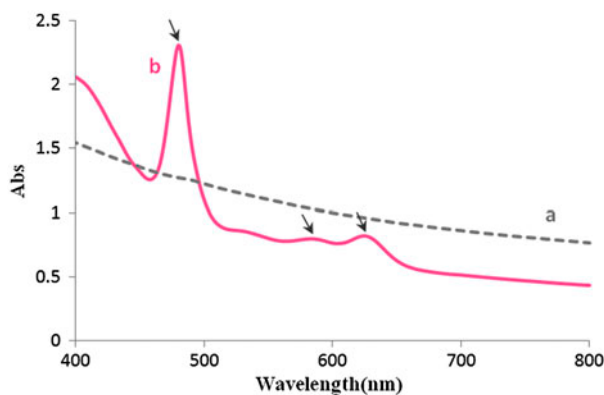


Figure 5. UV-vis spectra of: (a) $\text{Fe}_3\text{O}_4@\text{SiO}_2\text{-Im}$, (b) $\text{Fe}_3\text{O}_4@\text{SiO}_2\text{-Im}@\text{[MnT(4-OMeP)]}$.

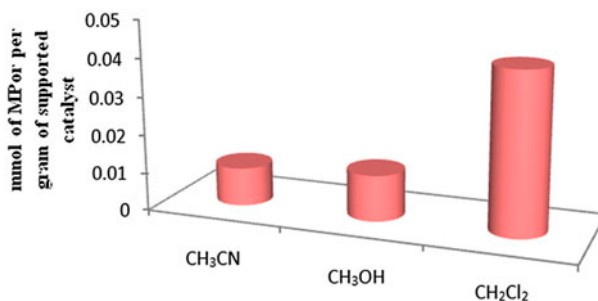


Figure 6. Effect of solvent on immobilization of Mn-porphyrin at room temperature.

3.2. Effect of various parameters on immobilization process of MPor on Imidazole functionalized $Fe_3O_4@SiO_2$ nanoparticles

3.2.1. Effect of solvent on metalloporphyrin immobilization. Effect of solvent on the immobilization of metalloporphyrin was studied by carrying out the reaction in various solvents (CH_2Cl_2 , CH_3CN , and CH_3OH) at room temperature. After 24 h, Fe_3O_4 nanoparticles were collected and the quantity of immobilized metalloporphyrins was calculated by measuring the amount of manganese ions using AAS. The results show that CH_2Cl_2 is a superior solvent for metalloporphyrin immobilization (figure 6), with less immobilized metalloporphyrin when the reaction was carried out under acetonitrile or methanol. This may be attributed to the coordination ability of these solvents to the metalloporphyrin, which competes with imidazole groups on the surface of Fe_3O_4 nanoparticles.

3.2.2. Effect of temperature on metalloporphyrin immobilization. To study the effect of temperature on the immobilization of Mn-porphyrin on Fe_3O_4 nanoparticles, the immobilization was carried out at various temperatures in dichloromethane, and the quantity of immobilized metalloporphyrins was calculated by measuring the manganese content of the supported catalyst using AAS. It was determined that at higher temperatures, the amount of immobilized metalloporphyrin increased (figure 7).

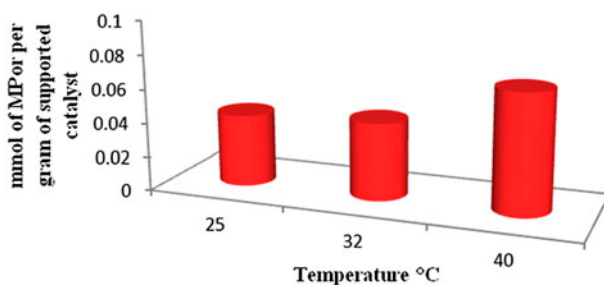
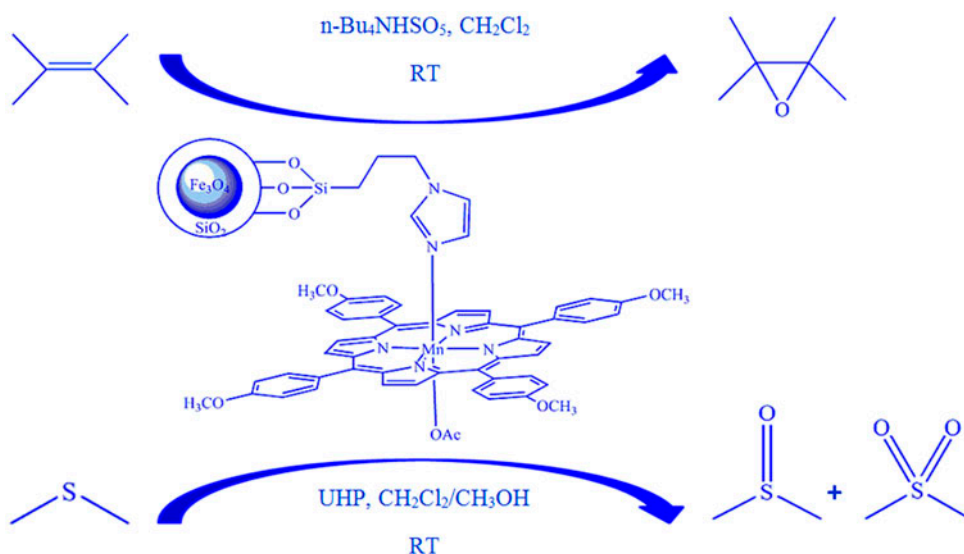


Figure 7. Effect of temperature on immobilization of Mn-porphyrin.



Scheme 2. Oxidation catalyzed by $\text{Fe}_3\text{O}_4@\text{SiO}_2\text{-Im}@\text{[MnT(4-OMeP)P]}$ (**1**).

3.3. Catalytic experiments

In this work, we report the catalytic activity of $[\text{MnT(4-OMeP)P}]\text{OAc}$ supported on imidazole functionalized $\text{Fe}_3\text{O}_4@\text{SiO}_2$ nanoparticles; $\text{Fe}_3\text{O}_4@\text{SiO}_2\text{-Im}@\text{[MnT(4-OMeP)P]}$ (**1**), in alkene epoxidation with tetra-*n*-butylammonium hydrogen monopersulfate ($n\text{-Bu}_4\text{NHSO}_5$) and sulfide oxidation in the presence of urea hydrogen peroxide (UHP) as an oxidant (scheme 2).

3.3.1. Alkene epoxidation catalyzed by $\text{Fe}_3\text{O}_4@\text{SiO}_2\text{-Im}@\text{[MnT(4-OMeP)P]}$. The catalytic performance of $\text{Fe}_3\text{O}_4@\text{SiO}_2\text{-Im}@\text{[MnT(4-OMeP)P]}$ was investigated in the oxidation reactions. First, epoxidation of cyclooctene was chosen as a model substrate to study the catalytic activity of heterogeneous catalyst **1**. Catalytic activity of manganese porphyrins is improved using a nitrogen base as cocatalyst [25]. Among the nitrogen bases,

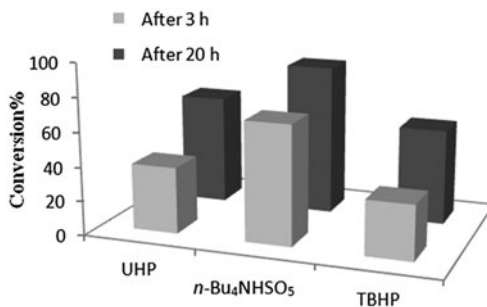


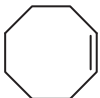
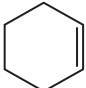
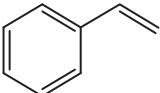
Figure 8. Effect of different oxidants on cyclooctene epoxidation catalyzed by $\text{Fe}_3\text{O}_4@\text{SiO}_2\text{-Im}@\text{[MnT(4-OMeP)P]}$.

which have been used as an axial ligand, imidazole exhibited higher activity in the epoxidation of alkenes. In this study, the $\text{Fe}_3\text{O}_4@\text{SiO}_2\text{-Im}$ not only is used as support, but also plays a role as an axial ligand. The optimum conditions used for the epoxidation of cyclooctene were catalyst:substrate:oxidant in a molar ratio of 1:285:570. In order to find suitable reaction conditions, the ability of different single oxygen donors such as tetra-*n*-butylammonium hydrogen monopersulfate (*n*- Bu_4NHSO_5), tert-butyl hydroperoxide (TBHP), and UHP was investigated in the epoxidation of cyclooctene at room temperature in CH_2Cl_2 as a solvent. The obtained results, which are summarized in figure 8, show that *n*- Bu_4NHSO_5 gives the highest conversion.

Under the same reaction conditions, the supported catalyst was used for epoxidation of different olefins with *n*- Bu_4NHSO_5 (table 1). $\text{Fe}_3\text{O}_4@\text{SiO}_2\text{-Im}@[\text{MnT}(4\text{-OMeP})\text{P}]$ is an efficient catalyst for epoxidation of alkenes in the presence of *n*- Bu_4NHSO_5 . In this heterogenized catalytic system, oxidation of cyclooctene produced cyclooctene oxide in 88.5% yield after 20 h. The cyclohexene was oxidized in high yield and selectivity to cyclohexene oxide and 2-cyclohexen-1-one was obtained in about 5% yield. The oxidation of styrene produced 61.2% of styrene oxide and 9% benzaldehyde was produced as by-product after 20 h. To study the influence of time in the oxidation process, the reactions were carried out in two different time intervals (3 and 20 h). As the results show in table 1 and figure 8, the best conversion was obtained after 20 h in terms of calculated turnover numbers (TON).

Adding small linear alcohols like CH_3OH with coordinating and hydrogen bonding abilities produces the metal-oxo ($\text{Mn}=\text{O}$) activated form of the catalyst more rapidly [26]. It is also believed that alcohols can act as general acid catalysts for the heterolytic cleavage of O–O bonds in the peroxy species, accelerating metal-oxo formation [27]. Better polarization in solution, more stability of the activated porphyrin, and longer lifetime occur in the presence of protic solvents. Therefore, epoxidation of cyclooctene was chosen as a model substrate to study the effect of solvent in the oxidation reaction. Using a solvent mixture, $\text{CH}_2\text{Cl}_2:\text{CH}_3\text{OH}$ with molar ratio of 1:1, in cyclooctene epoxidation with $\text{Fe}_3\text{O}_4@\text{SiO}_2\text{-Im}@[\text{MnT}(4\text{-OMeP})\text{P}]$ produced a 10–15% increase in epoxy yields (figure 9).

Table 1. Epoxidation of alkenes with *n*- Bu_4NHSO_5 catalyzed by $\text{Fe}_3\text{O}_4@\text{SiO}_2\text{-Im}@[\text{MnT}(4\text{-OMeP})\text{P}]^{\text{a}}$

Entry	Alkene	Conversion% ^{a,b}	Epoxide yield%	TON
1		88.5 ^a (70.2) ^c	88.5 ^a (70.2) ^c	252.8
2		87.3 ^{a,d} (79.4) ^{c,d}	82.3 ^a (74.8) ^c	249.4
3		70 ^{a,e} (58.5) ^{c,e}	61.2 ^a (51) ^c	200

^aReaction conditions: alkene (0.2 mmol), *n*- Bu_4NHSO_5 (0.4 mmol), catalyst (7×10^{-4} mmol), CH_2Cl_2 (1 mL), reaction time: 20 h.

^bDetermined by GC using chlorobenzene as an internal standard.

^cValues in parentheses were obtained after 3 h.

^dThe by-product is allylic ketone.

^eThe by-product is benzaldehyde.

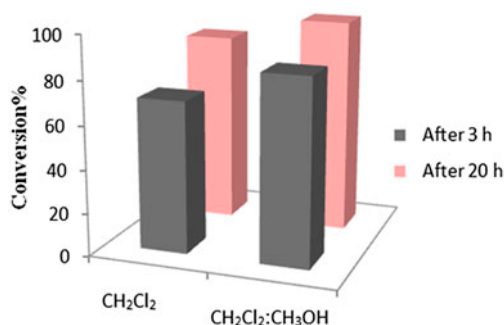


Figure 9. Effect of solvent on cyclooctene epoxidation catalyzed by $\text{Fe}_3\text{O}_4@\text{SiO}_2\text{-Im}@\text{[MnT(4-OMeP)]}$.

3.3.2. Sulfide oxidation catalyzed by $\text{Fe}_3\text{O}_4@\text{SiO}_2\text{-Im}@\text{[MnT(4-OMeP)]}$. The prepared catalyst was applied for oxidation of various sulfides in the presence of UHP under the same reaction conditions used in alkene epoxidation. As the results show in figure 10, the best conversions were obtained after 20 h in terms of calculated TON values. The oxidation reactions were carried out in solvent mixture; $\text{CH}_2\text{Cl}_2:\text{CH}_3\text{OH}$ with molar ratio of 1:1, and molar ratio of catalyst:sulfide:oxidant of 1:285:570.

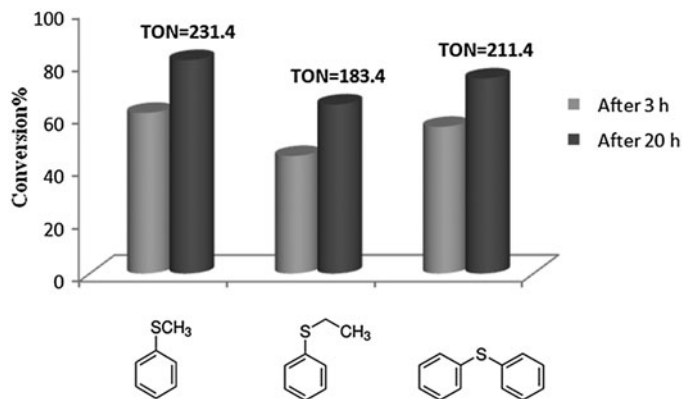


Figure 10. Oxidation of sulfides with UHP catalyzed by $\text{Fe}_3\text{O}_4@\text{SiO}_2\text{-Im}@\text{[MnT(4-OMeP)]}$.

Table 2. The results of catalyst recovery in cyclooctene epoxidation and methyl phenyl sulfide oxidation.

Run	Conversion (%) ^a	Mn leached (%) ^{a,c}	Conversion (%) ^b	Mn leached (%) ^{b,c}
1	99	1.8	81	1.5
2	90.1	0.9	75	0.8
3	87.6	0.7	73	0.6
4	80.3	0.4	68.5	d
5	79.9	d	68	d
6	79.2	d	67.5	d

^aReaction conditions: cyclooctene (0.2 mmol), *n*-Bu₄NHSO₅ (0.4 mmol), $\text{CH}_2\text{Cl}_2/\text{CH}_3\text{OH}$ (0.5 mL/0.5 mL), reaction time: 20 h.

^bReaction conditions: methyl phenyl sulfide (0.2 mmol), UHP (0.4 mmol), $\text{CH}_2\text{Cl}_2/\text{CH}_3\text{OH}$ (0.5 mL/0.5 mL), reaction time: 20 h.

^cDetermined by AAS.

^dNot detected.

3.3.3. Catalyst separation, reuse, and stability. Catalyst recovery and reuse are the two most important features for many catalytic processes. The homogeneous manganese porphyrin cannot be recovered even once; in contrast, the heterogeneous catalysts can be magnetically separated and reused multiple times without significant loss of catalytic activity. The stability of the magnetic nanocatalyst was monitored using a multiple sequential oxidation reaction. Since chemically modified Fe_3O_4 nanoparticles have high stability and Im-[MnT(4-OMeP)P]OAc coordination is quite strong, the catalyst resists cleavage in organic solvents. The reusability and the stability of the prepared catalyst were studied in repeated oxidation reactions. The catalyst was separated from the reaction mixture after each run, washed with CH_2Cl_2 and dried before being used. The results show that the catalyst can be reused six successive times for oxidation of substrates without any significant decrease in yield. The results of catalyst recovery in the epoxidation of cyclooctene with *n*-Bu₄NHSO₅ and the oxidation of methyl phenyl sulfide with UHP are presented in table 2. Also, the filtrates were collected for determination of Mn leaching by AAS analysis (table 2). The results show that, during recycling runs, some Mn is leached from the support. This observation and also decrease of catalytic efficiency after reusing for four runs may be due to release of surface-adsorbed or loosely coordinated Mn-porphyrin.

Comparing our results on oxidation reactions with those of other similar studies [17, 28–34] reveals that our catalytic system is superior to some of the previously reported catalysts in terms of catalytic activity (TON) and reaction conditions. The high TON of our catalyst compared to recently reported protocols [29–33] makes the $\text{Fe}_3\text{O}_4@\text{SiO}_2\text{-Im}@\text{[MnT(4-OMeP)P]}$ more attractive for oxidation of substrates. Compared with these nonporphyrin catalysts, our catalytic system exhibits high catalytic activity in terms of high TON.

Our heterogenized catalytic system can be recovered and reused in comparison with the homogeneous complexes [29–33]. Metal complexes are stabilized upon immobilization on solid supports because of the support environment. Also, the nanomagnet-supported catalyst, this work, can be separated with a magnet and reused several times without significant loss of activity.

According to the molar ratio of 1:285:570 for catalyst:substrate:oxidant which is carried out in this work, the amount of catalyst which is used in each run (0.01 g, containing 7×10^{-4} mmol of MnPor) is lower than that of previous work [28–34].

In addition, the effect of various parameters such as solvent and temperature on immobilization process of metalloporphyrin on imidazole functionalized $\text{Fe}_3\text{O}_4@\text{SiO}_2$ nanoparticles and also the effect of solvent and different oxidants on cyclooctene epoxidation have been investigated, while the influence of these factors was not examined previously [17]. The attractive features of this catalytic system such as low cost, easy preparation, simple recyclability, and reusability (considering the magnetic properties), high TON, mild reaction conditions make it particularly suitable for oxidation reactions.

4. Conclusions

$\text{Fe}_3\text{O}_4@\text{SiO}_2$ nanoparticles were synthesized and conventionally functionalized with imidazole. The nanoparticles were applied as support for the immobilization of manganese porphyrin and used as an efficient and reusable catalyst for alkene epoxidation and sulfide oxidation. The most important advantage of this heterogenized catalytic system is the simplicity of the catalyst separation in which the catalyst can be separated from the reaction

mixture by applying a magnet. Furthermore, the separation and reuse of the magnetic Fe₃O₄ nanoparticles were very effective and economical. The catalyst was consecutively reused about six times without significant loss of activity.

Disclosure statement

No potential conflict of interest was reported by the authors.

Funding

This work was financially supported by the Research Council of Sharif University of Technology.

References

- [1] M.A. Schiavon, Y. Iamamoto, O.R. Nascimento, M.D. Assis. *J. Mol. Catal. A: Chem.*, **174**, 213 (2001).
- [2] N. Bizaia, E.H. de Faria, G.P. Ricci, P.S. Calefi, E.J. Nassar, K.A.D.F. Castro, S. Nakagaki, K.J. Ciuffi, R. Trujillano, M.A. Vicente, A. Gil, S.A. Korili. *ACS Appl. Mater. Interfaces*, **1**, 2667 (2009).
- [3] A.K. Rahiman, S. Sreedaran, K.S. Bharathi, V. Narayanan. *J. Porous Mater.*, **17**, 711 (2010).
- [4] G.S. Machado, K.A.D. de Freitas Castro, F. Wypych, S. Nakagaki. *J. Mol. Catal. A: Chem.*, **283**, 99 (2008).
- [5] M. Halma, K.A.D. de Freitas Castro, V. Pre'vot, C. Forano, F. Wypych, S. Nakagaki. *J. Mol. Catal. A: Chem.*, **310**, 42 (2009).
- [6] A. Schätz, O. Reiser, W.J. Stark. *Chem. Eur. J.*, **16**, 8950 (2010).
- [7] K.V.S. Ranganath, J. Kloesges, A.H. Schäfer, F. Glorius. *Angew. Chem. Int. Ed.*, **49**, 7786 (2010).
- [8] K.V.S. Ranganath, F. Glorius. *Catal. Sci. Technol.*, **1**, 13 (2011).
- [9] M. Bagherzadeh, M.M. Haghdoost, A. Shahbazirad. *J. Coord. Chem.*, **65**, 591 (2012).
- [10] X.Q. Liu, Z.Y. Ma, J.M. Xing, H.Z. Liu. *J. Magn. Mater.*, **270**, 1 (2004).
- [11] S. Campelj, D. Makovec, M. Drogenik. *J. Magn. Mater.*, **321**, 1346 (2009).
- [12] K.E. Pelcher, M.R. Crawley, S. Banerjee. *Mater. Res. Express.*, **1**, 035014 (2014).
- [13] P.R. Cooke, J.R. Lindsay Smith. *J. Chem. Soc. Perkin Trans.*, **1**, 1913 (1994).
- [14] A.D. Adler, F.R. Longo, J.D. Finarelli, J. Goldmacher, J. Assour, L. Korsakoff. *J. Org. Chem.*, **32**, 476 (1967).
- [15] A.D. Adler, F.R. Longo, F. Kampas, J. Kim. *J. Inorg. Nucl. Chem.*, **32**, 2443 (1970).
- [16] J. Wang, Q.W. Chen, C. Zeng, B.Y. Hou. *Adv. Mater.*, **16**, 137 (2004).
- [17] M. Bagherzadeh, M.M. Haghdoost, F. Matloubi Moghaddam, B. Koushki Foroushani, S. Saryazdi, E. Payab. *J. Coord. Chem.*, **66**, 3025 (2013).
- [18] K.D. Kim, S.S. Kim, Y.H. Cho, H.T. Kim. *J. Ind. Eng. Chem.*, **13**, 1137 (2007).
- [19] J.H. Cai, J.W. Huang, P. Zhao, Y.J. Ye, H.C. Yu, L.N. Ji, J. Sol-Gel. *Sci. Technol.*, **50**, 430 (2009).
- [20] C. Yuan, Z. Huang, J. Chen. *Catal. Lett.*, **141**, 1484 (2011).
- [21] P. Das, A.R. Silva, A.P. Carvalho, J. Pires, C. Freire. *J. Mater. Sci.*, **44**, 2865 (2009).
- [22] M. Hesse, H. Meier, B. Zeeh. *Spektroskopische Methoden in der organischen Chemie* [Spectroscopic methods in organic chemistry], 6th Edn, Thieme, Stuttgart (2002).
- [23] R. Marschall, M. Sharifi, M. Wark. *Microporous Mesoporous Mater.*, **123**, 21 (2009).
- [24] Z. Dudas, C. Enache, G. Fagadar-Cosma, I. Armeanu, E. Fagadar-Cosma. *Mater. Res. Bull.*, **45**, 1150 (2010).
- [25] A. Aghabali, N. Safari. *J. Porphyrins Phthalocyanines.*, **14**, 335 (2010).
- [26] D. Mohajer, M. Abbasi. *Eur. J. Inorg. Chem.*, **2008**, 3218 (2008).
- [27] W. Nam, M.H. Lim, H.J. Lee, C. Kim. *J. Am. Chem. Soc.*, **122**, 6641 (2000).
- [28] M. Amini, M. Bagherzadeh, B. Eftekhari-Sis, A. Ellern, L.K. Woo. *J. Coord. Chem.*, **66**, 1897 (2013).
- [29] M. Amini, M. Bagherzadeh, Z. Moradi-Shoeili, D.M. Boghaei, A. Ellern, L.K. Woo. *J. Coord. Chem.*, **66**, 464 (2013).
- [30] M. Amini, M. Bagherzadeh, B. Atabaki, P. Gohari Derakhshandeh. *J. Coord. Chem.*, **67**, 1429 (2014).
- [31] M. Amini, M. Khaksar, D.M. Boghaei, M. Bagherzadeh, A. Ellern, L.K. Woo. *J. Coord. Chem.*, **67**, 2435 (2014).
- [32] M. Amini, M.M. Najafpour, M. Zare, M. Hołyńska, A. Nemati Moghaddam, M. Bagherzadeh. *J. Coord. Chem.*, **67**, 3026 (2014).
- [33] T. Heikkilä, R. Sillanpää, A. Lehtonen. *J. Coord. Chem.*, **67**, 1863 (2014).
- [34] X.-L. Tang, A.-Q. Ma, G.-Q. Cai, L.-G. Zhu. *J. Coord. Chem.*, **67**, 449 (2014).